

UV observations of the globular cluster M10 from HST and GALEX. The BSS population.¹

E. Dalessandro², F. R. Ferraro², B. Lanzoni², R. P. Schiavon³, R. W. O’Connell⁴ and G. Beccari⁵

² *Dipartimento di Astronomia, Università degli Studi di Bologna, via Ranzani 1, I-40127 Bologna, Italy*

³ *Astrophysics Research Institute, Liverpool John Moores University, Twelve Quays House, Egerton Wharf, Birkenhead CH41 1LD, UK*

⁴ *Astronomy Department, University of Virginia, P.O. Box 400325, Charlottesville, VA 22904, USA*

⁵ *ESO - European Southern Observatory, Karl-Swarzschild Str. 2, D-85748 Garching bei München, Germany*

03 May, 2013

ABSTRACT

We present a combination of high-resolution *Hubble Space Telescope* and wide-field ground-based and *Galaxy Evolution Explorer* data of the Galactic Globular Cluster M10 (NGC6254). By using this large data-set we determined the center of gravity of the cluster and we built its density profile from star counts over its entire radial extension. We find that the density profile is well reproduced by a single-mass King model with structural parameters $c = 1.41$ and $r_c = 41''$. We also studied the Blue Straggler Star population and its radial distribution. We count a total number of 120 BSS within the tidal radius. Their radial distribution is bimodal: highly peaked in the cluster center, decreasing at intermediate distances and rising again outwards. We discuss these results in the context of the *dynamical clock* scheme presented by Ferraro et al. (2012) and of recent results about the radial distribution of binary systems in this cluster.

Subject headings: binaries: close; blue stragglers; globular clusters: individual (M10, NGC6254); stars: evolution

¹Based on observations collected with the NASA/ESA *HST*, obtained at the Space Telescope Science Institute, which is operated by AURA, Inc., under NASA contract NAS5-26555. Also based on WFI observations collected at the European Southern Observatory, La Silla, Chile, within the observing program 69.D-0582.

1. INTRODUCTION

Blue Stragglers Stars (BSS) are a common population of any medium-size stellar aggregate such as open (Mathieu & Geller 2009) and globular clusters, as well as dwarf galaxies (Monelli et al. 2012). They are arguably the most common objects whose nature is not explainable in terms of the canonical evolution of a single star.

In an optical Color Magnitude Diagram (CMD) BSS appear hotter and brighter than Turn-Off (TO) stars, thus mimicking a sparse sequence of younger and more massive objects. Observational evidence (see for example Shara et al. 1997; Gilliland et al. 1998) showed that BSS are indeed more massive ($M \sim 1.2 - 2.0M_{\odot}$) than “normal” stars from the same cluster ($M \sim 0.8M_{\odot}$) thus they are thought to be the result of some mechanism responsible for increasing the masses of single stars.

Two main formation scenarios have been proposed over the years: the “collisional” scenario (COL-BSS; Hills & Day 1976) according to which BSS are the end-products of stellar mergers induced by collisions between single stars or binary systems; and the “mass-transfer scenario” (MT-BSS; McCrea 1964; Zinn & Searle 1976) in which BSS are the result of mass accretion between two stars in a binary system. These mechanisms are believed to work simultaneously within the same cluster (see the case of M30; Ferraro et al. 2009), with efficiencies that may be a function of environment (Ferraro et al. 1995; Davies et al. 2004). In particular, COL-BSS have higher probabilities to form in the cores of GCs where densities are incredibly high and so is the chance of collisions and interactions. On the contrary, the MT scenario is the dominant formation channel of BSS in very loose systems or in cluster outskirts, where binary systems are more likely to have evolved free of interactions with other stars.

Observational support to this idea comes from the results obtained from data for 47 Tucanae by Ferraro et al. (2006a; see also Lovisi et al. 2010 for M4), where a fraction of BSS has been found to have strong Carbon (C) and Oxygen (O) abundance anomalies probably due to mass transfer processes (Sarna & de Greve 1996).

Being 3-4 times more massive (independently of the formation mechanism) than the average cluster mass ($m \sim 0.3M_{\odot}$), BSS are heavily affected by dynamical friction and thus they are natural test particles to probe the internal dynamics of stellar aggregates. In particular their radial distribution (Ferraro et al. 1997) has been found to be an important tool to probe the efficiency of dynamical friction (Mapelli et al. 2006; Lanzoni et al. 2007a). This approach has been followed by our group over the past fifteen years leading to the construction of a large collection of BSS radial distributions (see Dalessandro et al. 2008a and references therein) over the full spatial extent of the clusters studied.

By using this data set, Ferraro et al. (2012; hereafter F12) introduced the definition of the “*dynamical clock*”, i.e. a measurement that provides an assessment of the dynamical age

of a cluster on the basis of the presence and the position of the minimum of its BSS radial distribution.

Following this interpretation, clusters with a flat radial distribution (ω Centauri - Ferraro et al. 2006b; NGC2419 - Dalessandro et al. 2008b; Palomar14 - Beccari et al. 2011) are dynamically young, so that the effect of dynamical friction is still not present. Clusters whose BSS distribution has a single peak at the center (M79 - Lanzoni et al. 2007b; M75 - Contreras Ramos et al. 2012; M30 - Ferraro et al. 2009; M80 - F12) are dynamically old, so that the most remote BSS already have drifted towards the cluster center. Finally intermediate dynamical-age clusters show a bimodal BSS radial distribution with a peak in the cluster center and another one towards the outer regions, thus defining a clear minimum in the distribution. The radial position of this minimum (r_{min}) has been found to be linked to the efficiency of the dynamical friction and to strongly correlate with the central relaxation time (F12).

In this work we present a photometric analysis of the GGC M10 (NGC 6254) with the aim of studying its structural parameters and the properties of its BSS population. The results will be interpreted in the framework of the scheme proposed by F12 and will be compared with previous results on M10's binary systems content and mass segregation profile (Beccari et al. 2010, hereafter B10; Dalessandro et al. 2011, hereafter D11).

2. DATA ANALYSIS

As suggested by Ferraro et al. (1997; 2004), since BSS are relatively warm stars ($T_{eff} \sim 7000 - 10000K$), the optimal way to observe them is at ultraviolet (UV) wavelengths, where they define a bright and well defined sequence that is easily distinguishable in the CMD. In fact in the wavelength regime between 1800\AA and 3500\AA , giants, that are the brightest objects at optical and near infrared (IR) bands, give a negligible contribution to the total light. Therefore, stellar crowding is negligible, which makes identification of hot stars very easy.

2.1. Observations and data reduction

We combined high resolution optical and UV images obtained with HST and optical and UV wide field images collected both from ground-based and space telescopes. In particular the data-set is composed of:

1. *high-resolution sample* – It consists of a combination of images obtained with the Advanced Camera for Surveys (ACS) and the Wide Field Camera 2 (WFPC2) on board the Hubble Space Telescope (HST). The WFPC2 data set (Prop. 6607, PI: F.R.Ferraro) has been already presented by Ferraro et al. (2003) and it consists of a series of images in the F255W, F336W and F555W filters.

This data-set has been supplemented by ACS optical images already used by B10 and D11. In addition, in order to minimize the impact of saturation on bright stars, we supplemented that catalogue with short exposure time images: two images in F606W and F814W with exposure time $t_{exp} = 7sec$ each (Prop: 10775, PI: Sarajedini).

As shown in Figure 1, the centre of the cluster is located in the Planetary Camera (PC) for the WFPC2 data-set and in the gap between the two chips of the ACS data-set.

2. *wide field sample* – It consists of UV wide-field images secured with the *Galaxy Evolution Explorer* (GALEX; Schiavon et al. 2012; Dalessandro et al. 2012) and optical ground-based wide-field images obtained with the Wide Field Imager (WFI) mounted at the 2.2m ESO-MPG telescope.

The GALEX data set (PI R.P. Schiavon, GI1 release) has been already presented by Schiavon et al. (2012) and it consists of two circular images of $\sim 1 \text{ deg}^2$, one obtained with the FUV channel and $t_{exp} = 1911sec$ and one with NUV channel with $t_{exp} = 25362sec$. These images are aligned and the core of the cluster is approximately located in the centre of the detectors.

The WFI data-set (Prop. 69.D-0582(A), PI Ortolani) is composed of 9 images in the I band, 6 with $t_{exp} = 30sec$ and 3 with $t_{exp} = 3sec$ and of 9 V band images, 6 with $t_{exp} = 50sec$ and 3 with $t_{exp} = 5sec$.

The photometric analysis has been carried out by using DAOPHOTII (Stetson et al. 1987) for all the images with the exception of the WFPC2 data-set for which ROMAFOT (Buonanno et al. 1983) has been adopted. For the full description of the photometric reduction procedure see Ferraro et al. (2003), B10 and Schiavon et al. (2012).

2.2. Astrometry and photometric calibration.

The catalogues obtained from each data-set were put on the absolute astrometric system using a large number of stars in common with the *Guide Star Catalogue* (GSC2.3) . First, we obtained the astrometric solution for each of the 8 WFI chips by using a third order poly-

nomial solution found by the CataXcorr package². Since the core regions of GC do not host astrometric standard stars, we used the stars in the WFI catalogue as secondary astrometric standards to extend the astrometric solution to the internal regions. All the stars in common with GALEX, and with the *high resolution sample* were then used as secondary astrometric standards. Several hundreds of them have been found in each step and this allowed us to find a very accurate astrometric solution with typical uncertainties of about 0.2'' in both right ascension (α) and declination (δ).

More than 200 stars in common with the publicly available "Photometric Standard Fields"³ catalogue (Stetson 2000) were used to calculate the color equations needed to transform the V and I WFI magnitude into the standard Johnson-Cousin photometric system. The ACS m_{F606W} and m_{F814W} magnitudes were calibrated respectively to V and I by using the stars in common with the WFI catalog. In particular, the best linear fits to the star distribution in the (V- m_{F606W} , V-I) or the (I- m_{F814W} , V-I) planes have been applied. The same approach has been adopted for the m_{F555W} WFPC2 magnitudes, while m_{F255W} and m_{F336W} have been calibrated to the STMAG photometric system by using the procedure and Zero-Points reported in Holtzman et al. (1995). The NUV ABMAG GALEX magnitudes have been converted to m_{F255W} by means of Equation 1 obtained by linearly fitting the stars in common in the ($m_{F255W} - NUV$, $m_{F255W} - V$) plane.

$$m_{F255W} = NUV + 0.02 \times (m_{F255W} - V) + 0.39 \quad (1)$$

The final catalogue is composed of all stars in the WFPC2 catalogue and those detected in the complementary ACS FOV (see Figure 1). It also includes the stars in the WFI catalogue and external to both the WFPC2 and ACS FOVs (Figure 2). Stars in the WFI catalogue and in common with GALEX have also a m_{F255W} magnitude.

2.3. Center of gravity and density profile.

We determined the center of gravity C_{grav} of M10 by averaging the positions α and δ of selected stars (see below) lying in the FOV of the WFPC2/Planetary Camera, as previously done in other works by our group (see Dalessandro et al. 2009 for example). We choose the center listed by Goldsbury et al. (2010) as initial guess for our iterative procedure (Montegriffo et al. 1995). In order to avoid spurious or incompleteness effects, we performed

²CataXcorr is a catalog cross-correlation software developed at the Bologna Observatory by P. Montegriffo

³<http://www3.cadc-ccda.hia-ihp.nrc-cnrc.gc.ca/community/STETSON/standards/>

three different measurements by using three sub-sample of stars respectively with $V < 19$, $V < 18.5$ and $V < 18$. The resulting C_{grav} is the average of three measurements thus obtained and it is located at $\alpha_{J2000} = 16^h57^m8^s.92$, $\delta_{J2000} = -4^\circ05'58''.07$ ($RA = 254.2871636$ $Dec = -4.0994655$). C_{grav} is located at $\sim 3.5''$ North-West from the one published by Goldsbury et al. (2010). We checked that this difference does not have any impact on the present analysis.

Taking advantage of the wide radial coverage of our photometric catalogue, which extends to distances from C_{grav} to $r \sim 1400''$, we constructed the star count density profile for the full cluster extent. We considered only stars with $14 < V < 19$ in the different data-sets (see Figure 3). We divided the total FOV in 28 concentric annuli centered on C_{grav} and reaching $r = 1300''$. Each annulus was then split in a number of sub-sectors (2 or 4 depending on the maximum angular coverage constrained by the WFI FOV). In each sub-sector the density was estimated as the ratio between star counts and area. The density assigned to a given annulus is the average of the densities computed in each sub-sector. The error assigned to each density measure is defined as the dispersion from the mean of the sub-sectors composing the considered annulus. The resulting density profile is shown in Figure 4. The three outermost points have almost the same density, defining a plateau, which was used to define the background density level ($\sim 2stars/arcmin^2$).

We performed a fit of the profile by using a single-mass King model (King 1966). The best fit model is shown in Figure 4 and the derived values of the core radius $r_c = 41 \pm 1''$, concentration $c = 1.41 \pm 0.03$ and tidal radius $r_t = 1053 \pm 100''^4$ are reported. The concentration obtained from our best-fit is in good agreement with those found by Harris (1996 - edition 2010; $c = 1.40$) and McLaughlin & Van der Marel (2005; $c = 1.41$), while r_c is slightly smaller than previous estimates ($r_c = 51''$ from Harris 1996; $r_c = 46.4''$ from McLaughlin & Van der Marel 2005) based on surface brightness profiles fitting. In an upcoming paper (Miocchi et al. 2013, in preparation), we will present a detailed comparison between observed density profiles and different theoretical models for a large sample of GGCs. For the case of M10, multi-mass King models and Wilson models (Wilson 1975) result in a significantly lower quality fit than the best solution described above.

⁴In the following analysis we will adopt as r_t the upper limit to the value obtained by the best fit King model.

3. SAMPLE DEFINITION

In order to study the BSS radial distribution, we need to select both BSS and at least one reference star population.

3.1. BSS selection

As explained in Section 2, CMDs involving UV photometry provide the best means for one to study the hottest stellar populations like BSS in GCs. In particular, the m_{F255W} filter from HST/WFPC2 allows for an excellent contrast between BSS and main sequence turnoff stars (see also Figure 1 in Ferraro 2006c). In order to make the selection between different samples as homogeneous as possible, we used the $(m_{F255W}, m_{F255W} - V)$ CMD. In this way, selection of BSS from WFPC2 and WFI/GALEX photometry was based on the same criteria.

As shown in Figures 5 and 6, in order to avoid possible contamination from TO and Sub Giant Branch (SGB) stars, we adopted a limiting magnitude $m_{F255W} = 20$ (that is ~ 1 mag brighter than the cluster TO). In addition, in order to limit the contamination from possible blends with the Red Giant Branch (RGB) stars, we restricted our sample to stars bluer than $(m_{F255W} - V) = 2.5$. The boxes shown in Figures 5 and 6 illustrate this selection. These limits have been fixed on the basis of the quality of both the WFPC2 and the WFI/GALEX NUV CMDs. With these criteria we selected 47 and 48 BSS in the WFPC2 and WFI/GALEX FOVs respectively.

The complementary ACS is the only catalogue for which we do not have UV band measurements. We guarantee the homogeneity of the BSS selection by translating the m_{F255W} magnitude cut into the V band. The adopted magnitude limit $m_{F255W} = 20$ corresponds to $V \sim 18$. We adopted this magnitude cut to select BSS in the ACS FOV. Also in this case, an additional constraint on the (V-I) color has been adopted ($(V - I) < 0.8$). In this way we selected 25 additional BSS in the complementary ACS FOV (Figure 7).

We obtained a rough estimate of the possible Galaxy field star contamination by counting the number of stars located in our catalogue at distances larger than r_t and lying in the adopted (V,V-I) selection box. We find only one object over an area of about 150 arcmin^2 (corresponding to $\sim 0.01 \text{ stars/arcmin}^2$).

3.2. The Reference populations

The selection of the RGB stars, adopted as first reference population, has been done in the optical CMDs where they are the brightest stars. In particular we selected all the stars with $13.8 < V < 17$ along the RGB mean ridge line (see Figure 7). With these limits we selected respectively 229, 203 and 538 RGBs in the WFPC2, ACS and WFI samples (open pentagons in Figure 7).

As it is possible to see in Figure 7, field stars describe a vertical sequence at $(V - I) \sim 1$ thus contaminating mainly the SGB and RGB sequences. As done for BSS we counted the number of field stars in the RGB region at $r > r_t$. We found 36 objects, resulting in an average density of $\sim 0.2stars/arcmin^2$. We took this fraction into account for the estimate of the populations ratios (Section 4).

We used as second reference population the Horizontal Branch (HB) stars. When possible, the selection was performed in the $(m_{F255W}, m_{F255W} - V)$ CMD as shown in Figures 5 and 6. We found in our sample 90 HBs in the WFPC2 FOV, 86 in ACS and 129 HB in GALEX/WFI. We count 3 field stars lying in the CMD in the HB selection area and at $r > r_t$ corresponding to an average density of $\sim 0.02stars/arcmin^2$.

In addition to the statistical decontamination of the selected populations, we looked for extra-galactic sources by matching our catalogue with the NASA Extragalactic Database (NED)⁵. A total of 14 sources has been found: 12 galaxies and 2 Quasars (QSOs) (see Figure 7 right panel). The Quasar [HGP92] 165429.30-040340.3 (source # 2 in the NED catalogue) is in the HB region (see also Figure. 6) and it has been removed from the HB population.

We identified three out of four known variable stars in M10 (Sawyer 1938; Arp 1955 and Voroshilov 1971): V1, V2 are respectively a foreground WUma and a background RRlyrae (von Braun et al. 2002), while V4 is an HB star in the instability strip. We could not match V3 with our catalogue, since it lies in one of the WFI gaps (Figure 2).

4. THE BSS RADIAL DISTRIBUTION.

In order to analyze the BSS radial distribution we first compared its cumulative radial distribution to those of the reference populations.

We took into account the effect of contamination by statistically decontaminating the se-

⁵<http://ned.ipac.caltech.edu/>

lected populations. In particular we divided the FOV in 5 concentric annuli centered on C_{grav} and for each of them we randomly subtracted a number of stars constrained by the average field densities quoted in the previous Sections. The cumulative radial distribution of the statistically decontaminated populations is shown in Figure 8. As apparent, BSS (solid line) are more centrally concentrated than RGBs and HBs (dashed and dotted lines respectively). We assessed the statistical significance of the observed difference between the radial distribution of the three populations by means of a Kolmogorov-Smirnov test. We found that BSS and HB have a probability $P=92\%$ (corresponding to $\sim 1.7\sigma$) to be extracted from different parent populations, and BSS and RGB have $P > 99.9\%$ (corresponding to a significance larger than 3σ).

For a more quantitative analysis, we divided the total FOV in the same five annuli used before. The number of stars of each decontaminated population are reported in Table 1. In each of them we estimated the ratio between the number of decontaminated BSS and reference population stars in each annulus ($N_{BSS}^{ann}/N_{ref}^{ann}$). The radial distribution is clearly bimodal (see Figure 9), strongly peaked in the central regions, decreasing at intermediate radii and rising again outwards. As expected for "normal" cluster populations, the number ratio between the reference populations N_{HB}/N_{RGB} does not show any peculiar and significant trend.⁶ As discussed in the Introduction, the BSS bimodal distribution is a common feature of most of the GCs studied so far (see F12).

As a further check we compared the distribution of the double normalized ratio (Ferraro et al. 1993):

$$R_{POP} = \frac{N_{POP}^{ann}}{N_{POP}^{tot}} / \frac{L_{samp}^{ann}}{L_{samp}^{tot}} \quad (2)$$

where L_{samp}^{ann} and L_{samp}^{tot} are the light sampled in each annulus and in the field covered by the observations, respectively (Table 1).

Figure 10 shows that the distributions of HB and RGB stars follow that of the cluster sampled light and $R_{HB/RGB} = 1$, as expected by stellar evolution theory (Renzini & Buzzoni 1989) for post-MS stars, while the distribution of R_{BSS} is bimodal. The normalized ratio at the cluster center is found to be $R_{BSS} \sim 1.8$, which is in good agreement with values found for the central peaks of other GGCs (F12). The minimum of the distribution is located at

⁶HB stars are mildly more centrally concentrated than RGBs for $r < 100''$ (Figure 9 and see also Figure 10). This is also observable looking at their relative cumulative radial distributions (Figure 8). However the statistical significance of this difference is relatively small, as highlighted earlier in this Section.

$r_{min} \sim 10.35r_c$. In the cluster outskirts the normalized ratio is $R_{BSS} \sim 1$, which is what one should expect to find for binary systems and their by-products evolved in isolation (see Section 5)

5. DISCUSSION.

Simple analytical models (Mapelli et al. 2004, 2006) have shown that the observed radial distribution of BSS is well reproduced by modeling the dynamical friction acting on the binary population. By using equation (1) in Mapelli et al. (2004; see also Binney & Tremaine 1987) and the best-fit King model obtained in Section 2.3, we estimated the distance at which a star as massive as $1.2M_\odot$ (estimated average mass for a BSS; Shara et al. 1997) would have already sunk into the cluster core because of dynamical friction. It is predicted to be $r \sim 11r_c$, nicely matching the observed minimum in the BSS radial distribution.

As clearly stated in F12, different BSS radial distributions are the observational evidence of different stages of the cluster dynamical history. As time passes, the distance from the cluster center at which dynamical friction has been effective on BSS (and their progenitors) increases, and so does the position of the minimum in the observed radial distribution. In particular, when mass segregation and dynamical friction start to segregate binaries (and their by-products) into the cluster centre, a central peak in the BSS distribution occurs. Since the action of dynamical friction and mass segregation progressively extends to larger and larger distances from the centre, the dip left by the massive objects sunk to the bottom of the potential becomes visible at progressively increasing radii. In the meanwhile, the most remote BSS are still evolving in isolation in the outer regions of the cluster with nearly the same initial frequency (this generates the rising branch of the observed bimodal BSS distributions). Hence because of the dynamical friction effect, the dip of the distribution progressively moves outward with increasing (dynamical) age of the cluster. In a highly evolved cluster we can expect that virtually all the binaries and their by-products (at any distance from the cluster centre) have sunk into the cluster core, thus generating a single central peak in the BSS radial distribution, as observed for example in NGC1904 (Lanzoni et al. 2007b).

F12 show that the BSS radial distribution is a good tool to rank the dynamical stage reached by stellar systems, thus allowing a direct measure of cluster dynamical age purely from observed properties. In F12, M10 is classified as a *Family II* GC. This family is populated by clusters with intermediate dynamical ages. In addition, the r_{min} value found for M10 positions it towards the dynamically older end of *Family II* clusters. F12 showed that the core relaxation time (as well as the half-mass relaxation time) is a linear function of r_{min} .

This behavior allowed the definition of the "dynamical clock": clusters with relaxation times of the order of the age of the Universe show no sign of BSS segregation (hence the radial distribution is flat and r_{min} is not defined). For decreasing relaxation times the radial position of the minimum increases progressively.

The structural parameters obtained in the present work for M10 are slightly different from those adopted by F12. Following the approach used by the authors, we detail here the calculations for the core relaxation time and the position of M10 in the "dynamical clock" scheme on the basis of the results obtained in Section 2.3.

The core relaxation time (t_{rc}) was computed by using equation (10) in Djorgovski (1993):

$$t_{rc} = 1.491 \times 10^7 \text{yr} \times \frac{0.5592}{\ln(0.4N_{\star})} \frac{\sqrt{\rho_{M,0}}}{\langle m_{\star} \rangle} r_c^3, \quad (3)$$

where N_{\star} is the total number of stars in the cluster, $\rho_{M,0}$ is the central mass density in M_{\odot}/pc^3 and r_c is the core radius in pc. The values quoted in Djorgovski (1993) for a number of parameters were adopted, namely: the average stellar mass $\langle m_{\star} \rangle = 0.3M_{\odot}$, the stellar mass-to-light ratio in the V -band $M/L_V = 3$, the Sun V -band absolute magnitude $M_{\odot V} = 4.79$. The number of stars N_{\star} has been obtained as the ratio between the total cluster mass M_{tot} and $\langle m_{\star} \rangle$. M_{tot} has been calculated by using the M/L_V value quoted above, a bolometric correction factor for the V -band of 1.4 and the total luminosity L_V . The latter has been derived from the integrated V magnitude of the cluster $V_t = 6.60$ (Harris 1996), and the distance modulus $(M - m)_0 = 13.38$ and reddening $E(B - V) = 0.28$ quoted in Ferraro et al. (1999). The central mass density has been obtained as $\rho_{M,0} = \mu_V / (p \times r_c)$, where μ_V is the central surface brightness in L_{\odot}/pc^2 , p is a parameter which depends on the cluster King concentration c as in eq. (6) of Djorgovski (1993). To compute these parameters we used the $\mu_V = 17.70$ mag/arcsec² quoted by Harris (1996) and corrected for extinction, and the concentration ($c = 1.41$) and core radius ($r_c = 41''$) obtained from the best fit King model.

In Figure 11, we highlight the new position of M10 in the $(t_{rc}/t_H, r_{min})$ logarithmic plane. As already discussed, M10 represents together with a few other GCs, a sort of bridge between *Family II* and *Family III* (triangles Figures 12). In fact r_{min} is quite distant from the cluster center, but the BSS radial distribution is still bimodal.

In recent studies about both the mass segregation profile (B10) and the radial distribution of binary stars (D11), we have obtained similar results to the ones reported in the present work. In particular the radial distributions of binary stars and BSS show a very similar behavior at least at distances in which binaries have been analyzed ($r < 300''$). Indeed they both show clear evidence that in M10 energy equipartition has been achieved and heavier stars are moving on inner orbits.

We thank the anonymous referee for the careful reading and useful comments that improved the presentation of this work. This research is part of the project *COSMIC-LAB* (<http://www.comic-lab.eu>) funded by the *European Research Council* (under contract ERC-2010-AdG-267675). RPS acknowledges support from the Gemini Observatory, which is operated by the Association of Universities for Research in Astronomy, Inc., on behalf of the international Gemini partnership of Argentina, Australia, Brazil, Canada, Chile, and the United States of America.

REFERENCES

- Arp H. C., 1955, *AJ*, 60, 317
- Beccari G., Pasquato M., De Marchi G., Dalessandro E., Trenti M., Gill M., 2010, *ApJ*, 713, 194 (B10)
- Beccari G., Sollima A., Ferraro F. R., Lanzoni B., Bellazzini M., De Marchi G., Valls-Gabaud D., Rood R. T., 2011, *ApJ*, 737, L3
- Binney, J., Tremaine, S. 1987, Princeton, NJ, Princeton University Press, 1987
- Contreras Ramos, R., Ferraro, F. R., Dalessandro, E., Lanzoni, B., & Rood, R. T. 2012, *ApJ*, 748, 91
- Dalessandro E., Lanzoni B., Ferraro F. R., Rood R. T., Milone A., Piotto G., Valenti E., 2008a, *ApJ*, 677, 1069
- Dalessandro E., Lanzoni B., Ferraro F. R., Vespe F., Bellazzini M., Rood R. T., 2008b, *ApJ*, 681, 311
- Dalessandro, E., Beccari, G., Lanzoni, B., et al. 2009, *ApJS*, 182, 509
- Dalessandro, E., Lanzoni, B., Beccari, G., et al. 2011, *ApJ*, 743, 11 (D11)
- Dalessandro, E., Schiavon, R. P., Rood, R. T., et al. 2012, *AJ*, 144, 126
- Davies, M. B., Piotto, G., & de Angeli, F. 2004, *MNRAS*, 349, 129
- Djorgovski, S. 1993, in *ASPC Conf. Ser. 50, Structure and Dynamics of Globular Clusters*, ed. S. G. Djorgovski & G. Meylan (San Francisco: ASP), 373D
- Ferraro, F. R., Fusi Pecci, F., & Bellazzini, M. 1995, *A&A*, 294, 80

- Ferraro, F. R., Paltrinieri, B., Fusi Pecci, F., et al. 1997, *A&A*, 324, 915
- Ferraro F. R., Messineo M., Fusi Pecci F., de Palo M. A., Straniero O., Chieffi A., Limongi M., 1999, *AJ*, 118, 1738
- Ferraro F. R., Sills A., Rood R. T., Paltrinieri B., Buonanno R., 2003, *ApJ*, 588, 464
- Ferraro, F. R., Beccari, G., Rood, R. T., et al. 2004, *ApJ*, 603, 127
- Ferraro F. R., et al., 2006a, *ApJ*, 647, L53
- Ferraro F. R., Sollima A., Rood R. T., Origlia L., Pancino E., Bellazzini M., 2006b, *ApJ*, 638, 433
- Ferraro, F. R. 2006c, arXiv:astro-ph/0601217
- Ferraro F. R., et al., 2009, *Natur*, 462, 1028
- Ferraro, F.R. et al., 2012, *Nature*, 492, 393
- Gilliland R. L., Bono G., Edmonds P. D., Caputo F., Cassisi S., Petro L. D., Saha A., Shara M. M., 1998, *ApJ*, 507, 818
- Goldsbury R., Richer H. B., Anderson J., Dotter A., Sarajedini A., Woodley K., 2010, *AJ*, 140, 1830
- Harris, W.E. 1996, *AJ*, 112, 1487 (2010 revision)
- Hills J. G., Day C. A., 1976, *ApL*, 17, 87
- Holtzman J. A., Burrows C. J., Casertano S., Hester J. J., Trauger J. T., Watson A. M., Worthey G., 1995, *PASP*, 107, 1065
- King I. R., 1966, *AJ*, 71, 64
- Lanzoni B., Dalessandro E., Ferraro F. R., Mancini C., Beccari G., Rood R. T., Mapelli M., Sigurdsson S., 2007a, *ApJ*, 663, 267
- Lanzoni, B., Sanna, N., Ferraro, F. R., et al. 2007b, *ApJ*, 663, 1040
- Lovisi L., et al., 2010, *ApJ*, 719, L121
- McLaughlin D.E., van der Marel R.P., 2005, *ApJSS*, 161, 304
- Mapelli M., Sigurdsson S., Ferraro F. R., Colpi M., Possenti A., Lanzoni B., 2006, *MNRAS*, 373, 361

- Mapelli M., Sigurdsson S., Colpi M., Ferraro F. R., Possenti A., Rood R. T., Sills A., Beccari G., 2004, *ApJ*, 605, L29
- Mathieu, R. D., & Geller, A. M. 2009, *Nature*, 462, 1032
- McCrea W. H., 1964, *MNRAS*, 128, 147
- Monelli, M., Cassisi, S., Mapelli, M., et al. 2012, *ApJ*, 744, 157
- Montegriffo P., Ferraro F. R., Fusi Pecci F., Origlia L., 1995, *MNRAS*, 276, 739
- Renzini A., Buzzoni A., 1986, *ASSL*, 122, 195
- Sarna M. J., De Greve J.-P., 1996, *QJRAS*, 37, 11
- Sawyer H. B., 1938, *PDDO*, 1, 57
- Schiavon R. P., et al., 2012, *AJ*, 143, 121
- Shara M. M., Saffer R. A., Livio M., 1997, *ApJ*, 489, L59
- Stetson P. B., 2000, *PASP*, 112, 925
- von Braun K., Mateo M., Chiboucas K., Athey A., Hurley-Keller D., 2002, *AJ*, 124, 2067
- Voroshilov Y. V., 1971, *ATsir*, 623, 7
- Wilson C. P., 1975, *AJ*, 80, 175
- Zinn R., Searle L., 1976, *ApJ*, 209, 734

r_{int}	r_{ext}	N_{BSS}	N_{RGB}	N_{HB}	$L_{smp}^{ann}/L_{smp}^{tot}$
0''	50''	43	183	78	0.24
50''	150''	46	328	125	0.43
150''	300''	16	171	47	0.20
300''	550''	3	80	23	0.10
550''	1150''	4	24	7	0.03

Table 1: Decontaminated number counts of BSS, RGB and HB stars and fractions of sampled light.

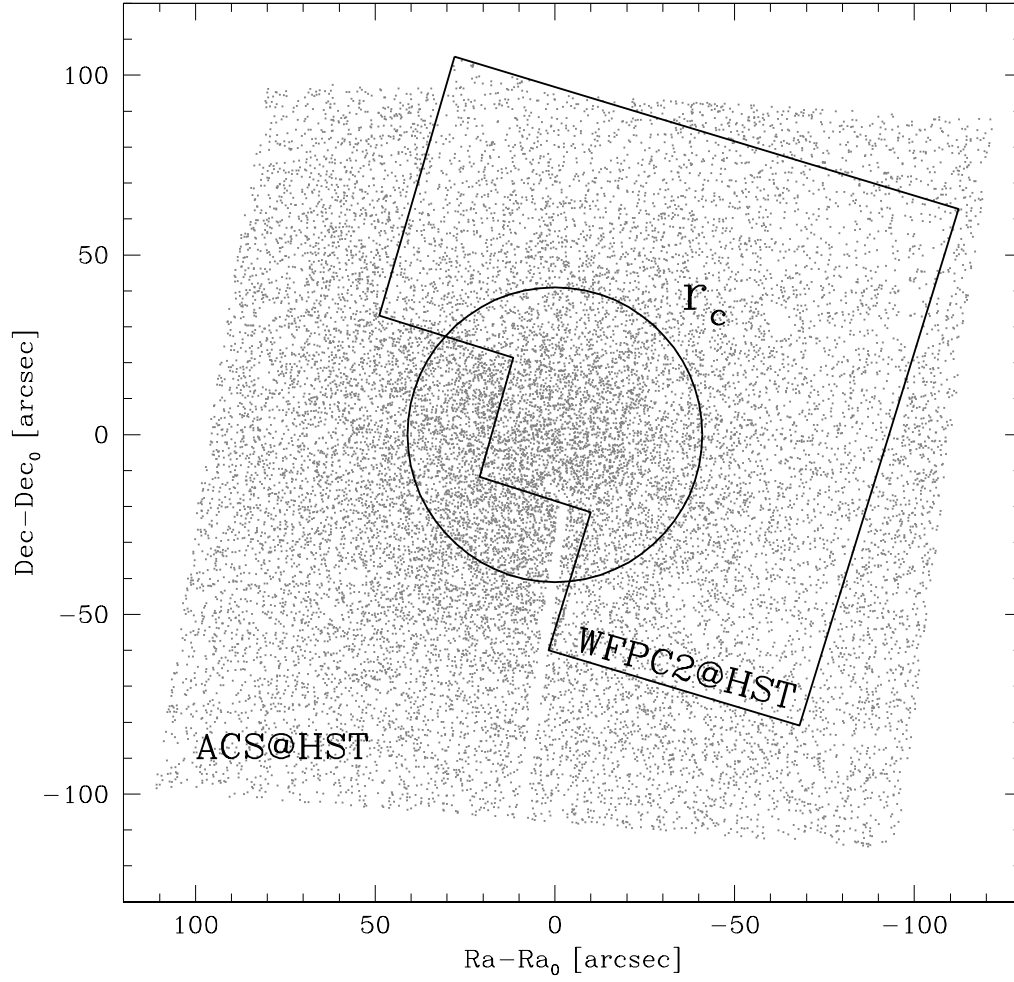


Fig. 1.— Map of the WFPC2 and ACS data. The black circle indicates the cluster core radius r_c (Section 2.3).

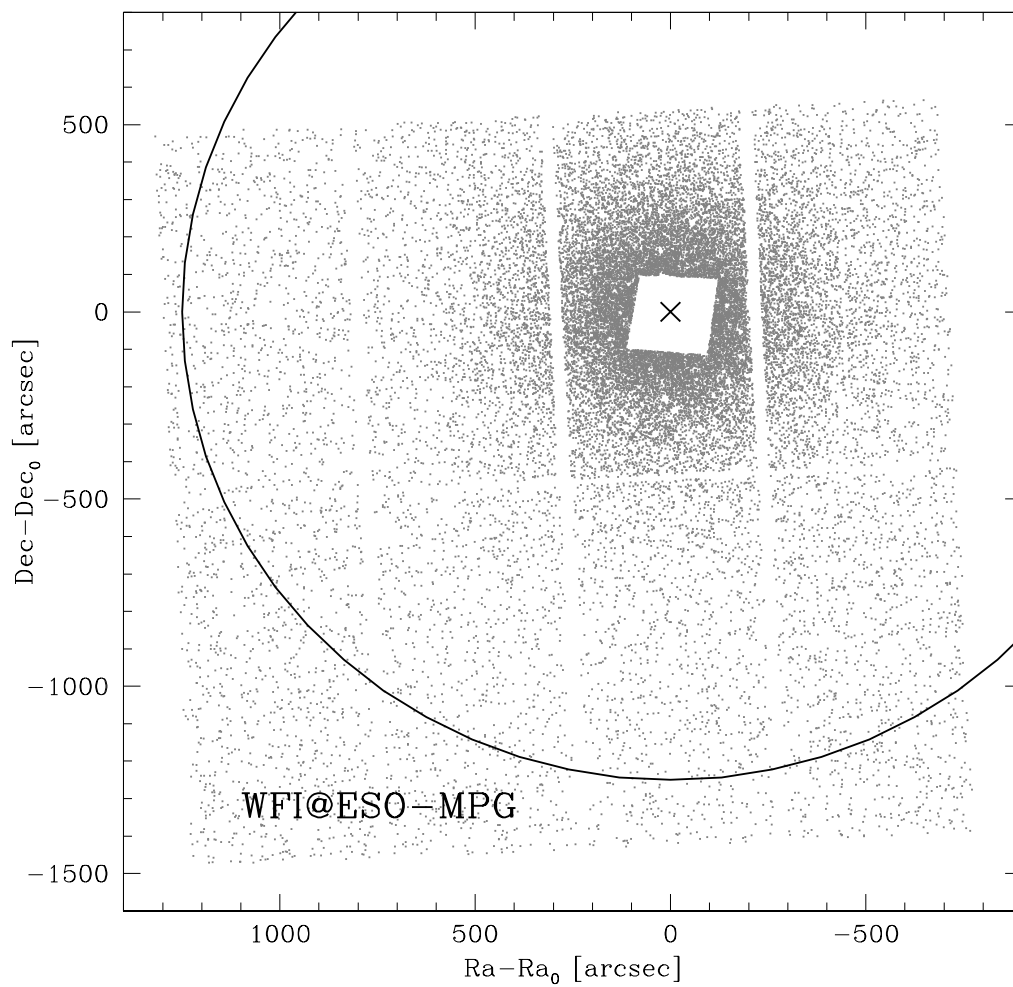


Fig. 2.— Map of the WFI data. The blank area corresponds to the ACS and WFPC2 FOVs. The black circle indicates the tidal radius r_t of M10 (see Section 2.3).

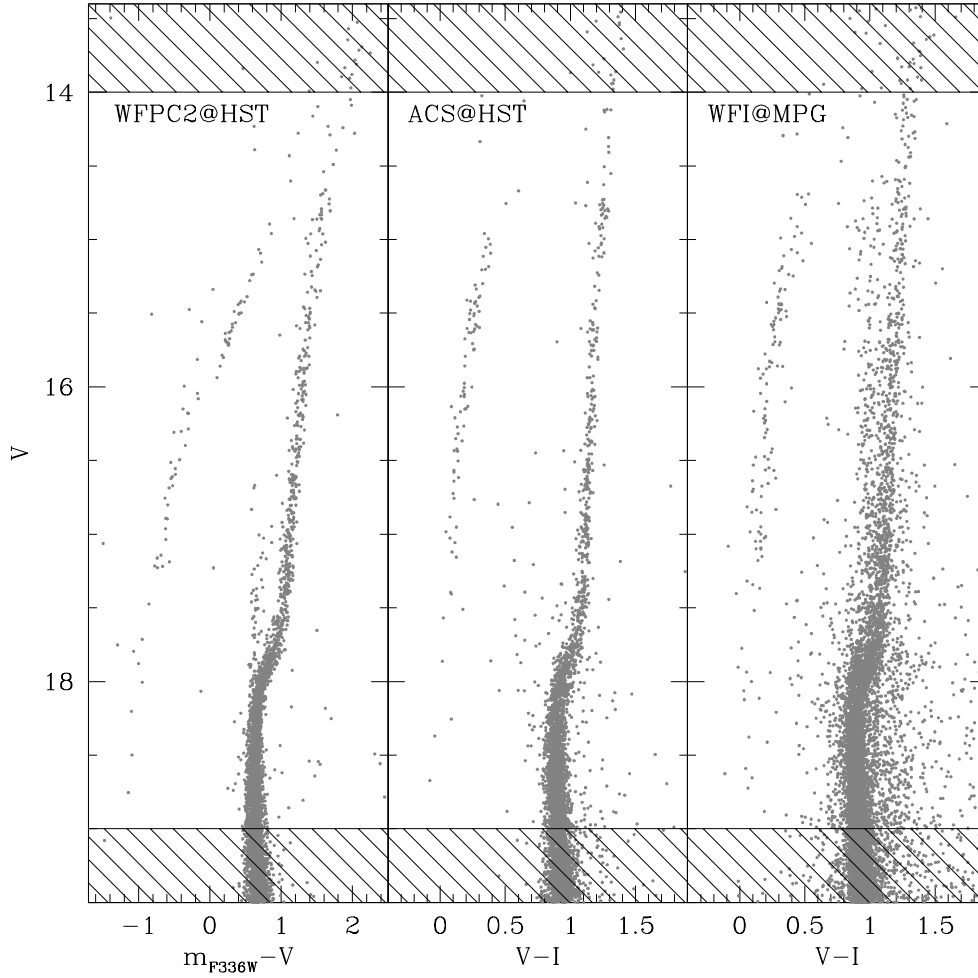


Fig. 3.— Optical CMDs of the WFPC2, ACS and WFI samples. The shaded regions ($V < 14$ and $V > 19$) delimit the samples excluded from the density profile calculation. In the rightmost panel only stars with $r < r_t$ are plotted.

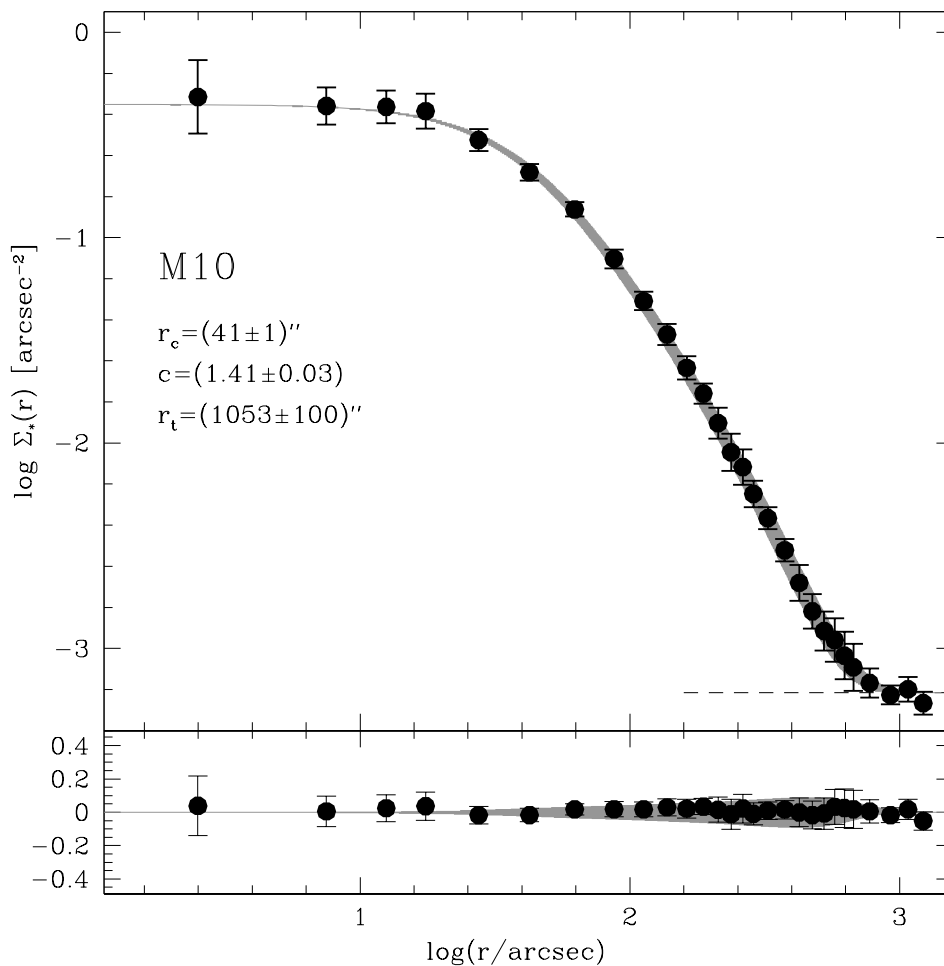


Fig. 4.— Observed surface density profile (black dots), based on counts of all cataloged stars with $14 < V < 19$. The filled grey region represents the area defined by the best-fit King model and the relative errors on the structural parameters. The dashed line indicates the measured level of the background. The parameters of the King model (core radius and concentration) and relative uncertainties are indicated in the figure. The lower panel shows the residuals in each radial bin.

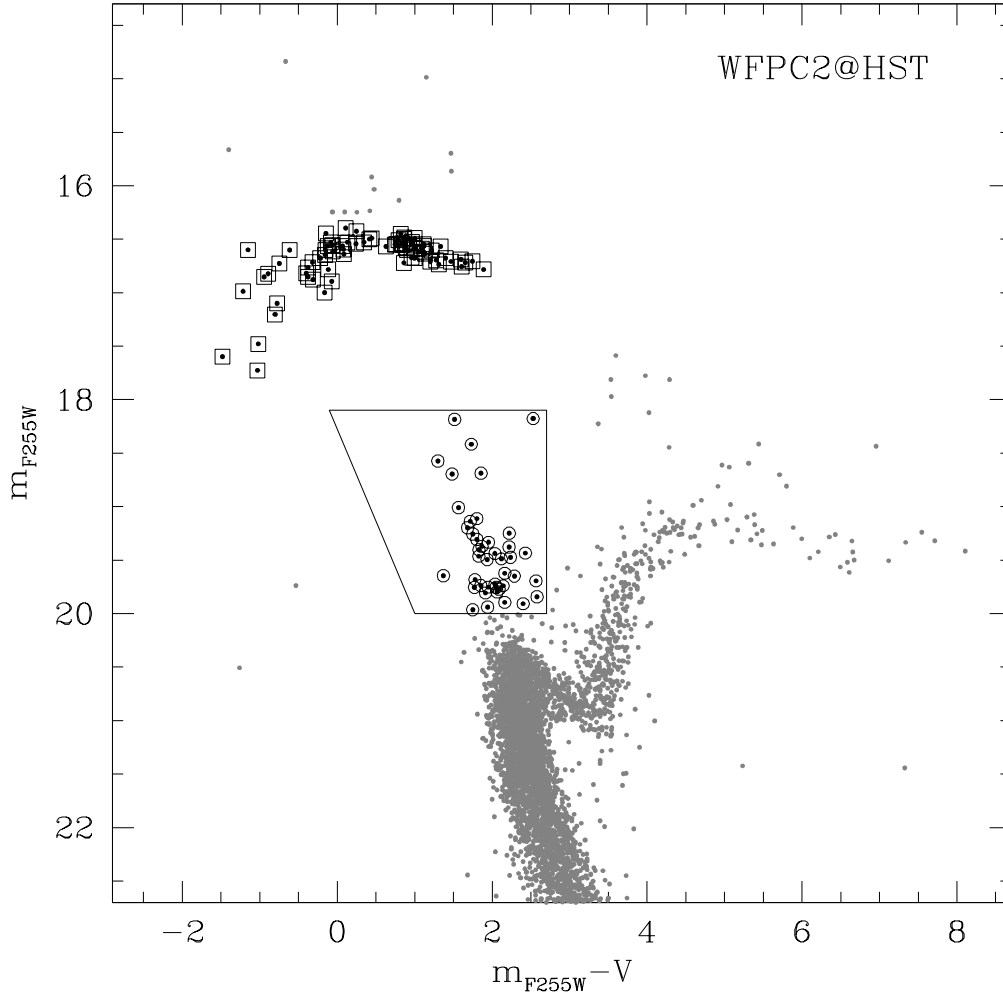


Fig. 5.— UV CMD of the WFPC2 sample. The box shows the magnitude and color limits defined for the BSS selection in this photometric plane. Open circles are the selected BSS, open squares are HBs.

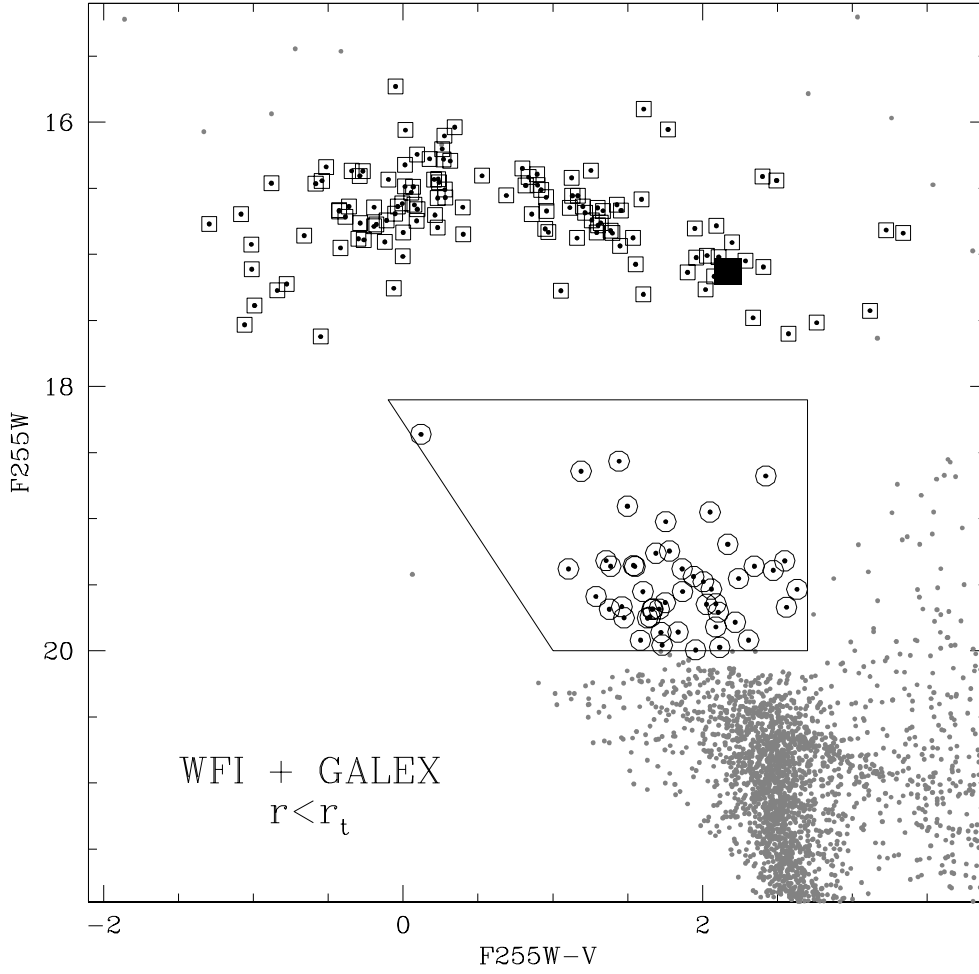


Fig. 6.— As Figure 5, but for the WFI/GALEX sample at $r < r_t$. The large solid square marks the location of the Quasar [HGP92] 165429.30-040340.3.

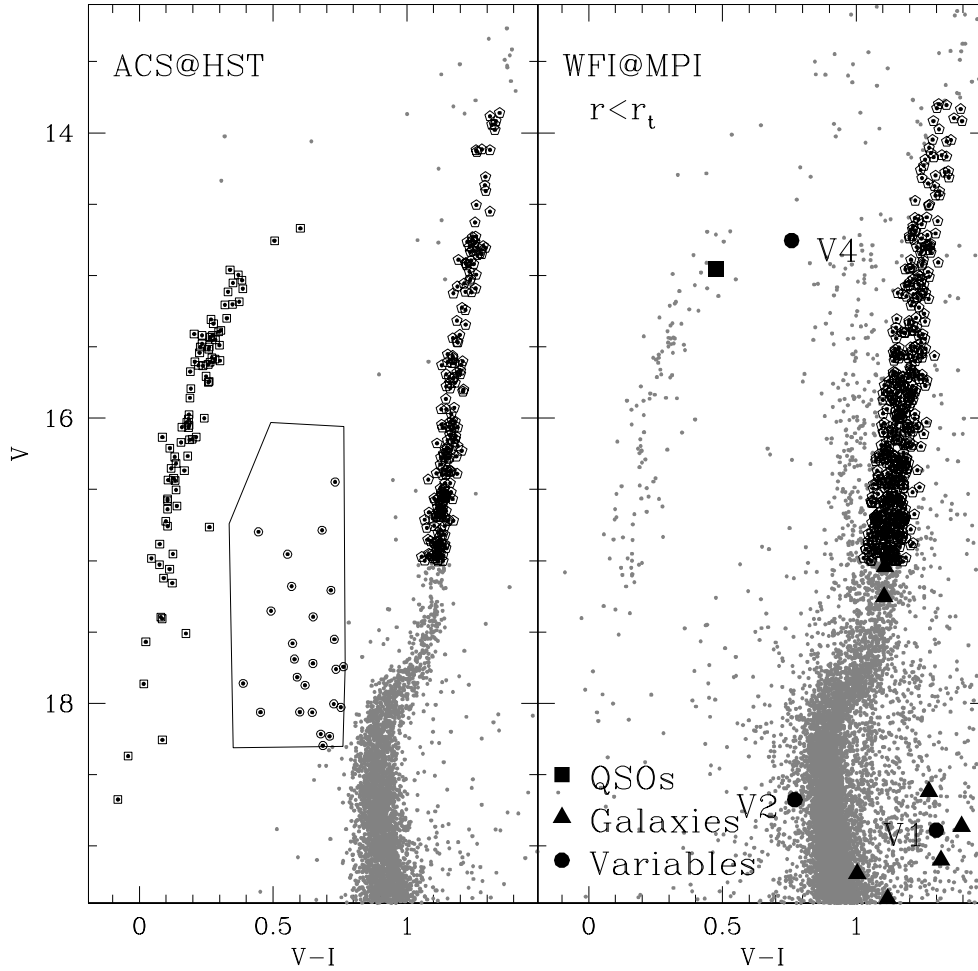


Fig. 7.— Optical CMDs of the ACS and WFI samples, on the left and right panel respectively. The box in the left panel defines the fiducial region for BSS selection in the optical plane (see for details Section 3). As in Figure 5, open circles are BSS and opens squares are HBs. Open pentagons are RGB stars. Quasars, galaxies and variables identified in literature (Section 3.2) are also highlighted with in the right panel as solid squares, triangles and circles, respectively.

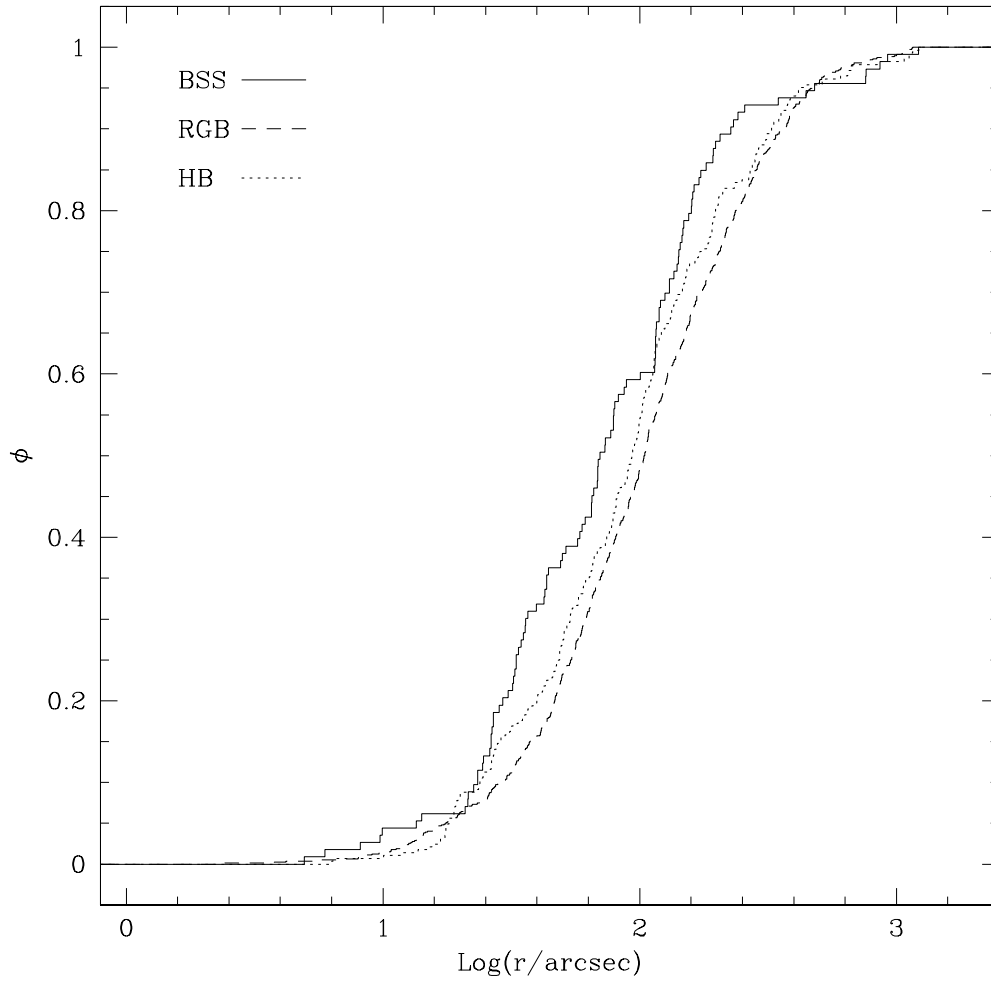


Fig. 8.— Cumulative radial distribution of the statistically decontaminated populations.

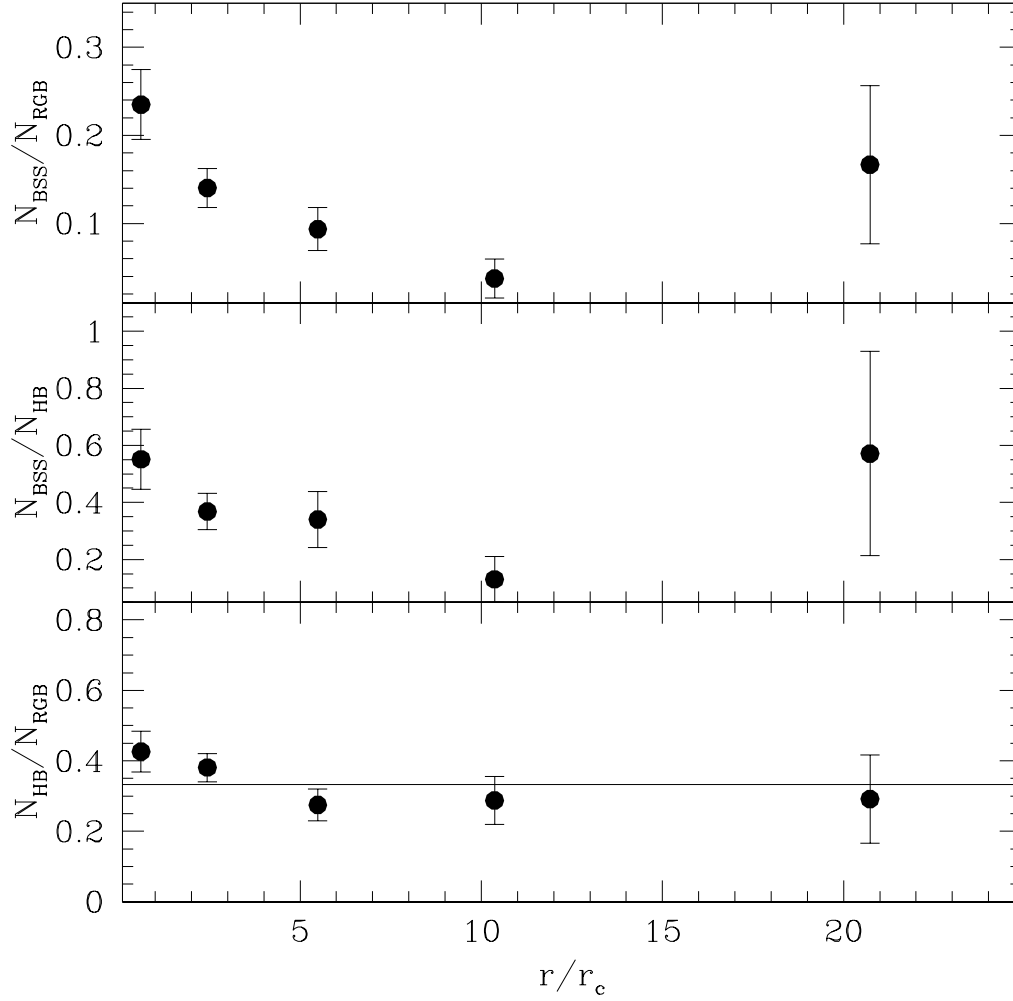


Fig. 9.— From top to bottom, N_{BSS}/N_{RGB} , N_{BSS}/N_{HB} and N_{HB}/N_{RGB} as a function of the distance from C_{grav} normalized to $r_c = 41''$. The solid line in the bottom panel represents the average value of N_{HB}/N_{RGB} for the entire cluster extension.

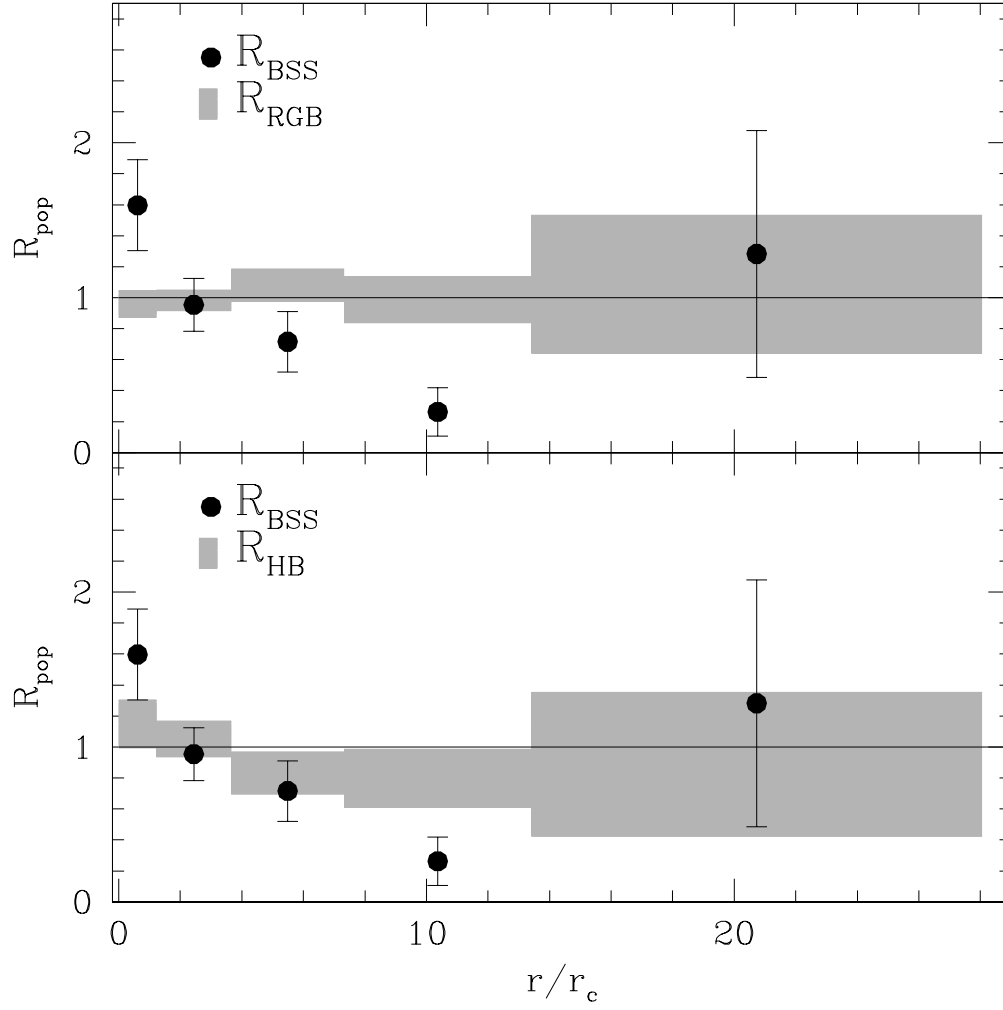


Fig. 10.— Radial distribution of the double normalized ratios of the BSS (black dots), RGB (upper panel) and HB (lower panel).

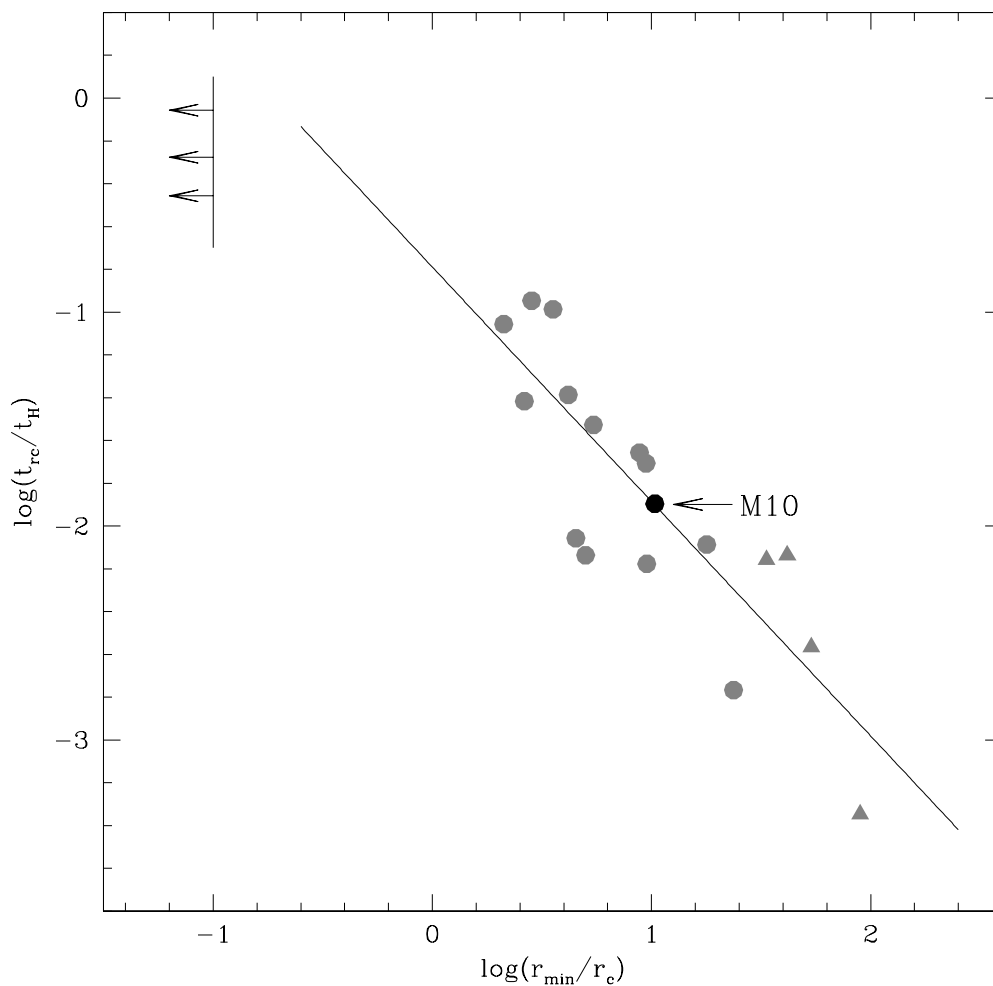


Fig. 11.— The relaxation time at the cluster centre (t_{rc}) normalized to the age of the Universe ($t_H = 13.7$ Gyr) as a function of r_{\min}/r_c . This plot is the same as Figure 4 of F12. The dynamically young clusters, for which it is not possible to define a minimum in the distribution, are shown as lower limit arrows at $r_{\min} = 0.1$. Grey circles are clusters classified as *Family II* in F12. M10 belongs to this family and its position has been highlighted in black. Triangles are the dynamically old clusters (*Family III*).

